Clays and Clay Minerals, Vol. 62, No. 4, 324–335, 2014.

MINERALOGICAL CHARACTERIZATION OF Ni-BEARING SMECTITES FROM NIQUELÂNDIA, BRAZIL

Eliana Satiko Mano[1,*], Laurent Caner[2], Sabine Petit[2], Arthur Pinto Chaves[1], and André Sampaio Mexias[3]

[1] Escola Politécnica, Universidade de São Paulo. Av. Prof. Mello Moraes 2.373, 05508-900, São Paulo, Brazil
[2] Université de Poitiers, CNRS IC2MP-HydrASA UMR 7285, Poitiers, France
[3] Universidade Federal do Rio Grande do Sul, Instituto de Geociências, UFRGS, Campus do Vale Av. Bento Gonçalves, 9500 - Porto Alegre - RS - Brazil

Abstract—Nickel-lateritic ore is the most common source of nickel in Brazil. The Niquelândia deposit, located in State of Goias, is one of the most famous deposits due to the large amounts of nickel associated with both oxidized and mainly silicated ores. The terms oxidized and silicated ores are used to specify two different ores formed exclusively by oxides and silicate (clay) minerals, respectively. The aim of the present study was to characterize thoroughly the silicated ore to identify the Ni-bearing clay minerals and their crystal chemistry in support of developing a better mineral-processing method or optimizing the current one to improve Ni recoveries. X-ray diffraction, chemical analyses, scanning electron microscopy, and Fourier transform infrared (FTIR) spectroscopy demonstrated that nickel is associated with Ni-rich stevensite and to a lesser extent with Fe-rich montmorillonite. The crystal chemistry performed by FTIR spectroscopy revealed that Ni is present in the octahedral positions, substituting for Mg or Fe, which results in significant chemical and layer-charge heterogeneity in the samples. This heterogeneity seems to be responsible for reduction in Ni recoveries during the hydrometallurgical process.

Key Words—Clay Minerals, Crystal Chemistry, Fe-montmorillonite, Nickel, Smectite, Stevensite.

INTRODUCTION

Nickel is important as a metal or as an alloying element in steels because of its low rate of oxidation and consequent resistance to corrosion. In nature, Ni is associated with sulfides and lateritic deposits. According to Dalvi *et al.* (2004), 70% of nickel worldwide is contained in lateritic deposits, and production of Ni-laterites increased from 140 kt/year to 1200 kt/year between 1950 and 2003. For this reason, extensive research into Ni-bearing clay minerals has been carried out. Nickel is associated with a wide variety of clay minerals such as serpentine, talc/kerolite/pimelite, and smectite.

Nickel exhibits a specific geochemical affinity for mantle-derived (mafic and ultramafic) rocks (Christidis and Mitsis, 2006). Mafic and ultramafic intrusions were responsible for the formation of the Niquelândia ultrabasic massif during the Archean period (Marini *et al.*, 1984). The combination of relief and seasonal alternations of large and small amounts of precipitation led to intense weathering of dunites, peridotites, and pyroxenites and to the formation of clay minerals.

Previous mineral characterization studies conducted at Niquelândia have indicated that the nickel is associated with a mixture of di- and trioctahedral smectites and talc (Bosio *et al.*, 1975; Brindley and de Souza, 1975; de Souza *et al.*, 1978; Colin *et al.*, 1985, 1990; Decarreau *et al.*, 1987; Oliveira, 1990; Coelho *et al.*, 2000; Raous *et al.*, 2013). Ni-bearing smectite is one of the secondary phases formed during low-temperature weathering processes of ultrabasic rocks – these smectites contain Fe^{3+} as the main octahedral cation with small amounts of Ni, ~<0.4 atoms per half formula unit (p.h.f.u.) (Bosio *et al.*, 1975; Gaudin *et al.*, 2004a). Nickel grades were observed to vary from 10 to 84% of occupancy in the octahedral sites of trioctahedral smectites in Niquelândia (Colin *et al.*, 1990). A Ni-rich stevensite has also been reported from Othrys, Greece (Christidis and Mitsis, 2006). The complex crystal chemistry of the clay minerals in Niquelândia may be the cause of significant variability in the ores which affects the recovery rates of Ni from the hydrometallurgical process. In the present study, the clay minerals in the silicated ore were characterized, focusing on the Ni-stevensite and Fe/Ni-montmorillonite. A detailed characterization of the Ni-bearing clay minerals in the samples, including the variability in the silicated ores, will help us to understand smectite formation and will provide pathways for improving Ni recovery from the hydrometallurgical process.

MATERIALS AND METHODS

The Niquelândia deposit is located in the State of Goias, central Brazil (Figure 1). The relief seen at Niquelândia reveals dunites and peridotites making up an old plateau covered by silcrete; pyroxenites are found in valley regions. Different parent rocks are responsible for different grades (high, intermediate, and low) of Ni in the silicated ore. In order to characterize these three

* E-mail address of corresponding author:
elli_mano@hotmail.com
DOI: 10.1346/CCMN.2014.0620406

https://doi.org/10.1346/CCMN.2014.0620406 Published online by Cambridge University Press

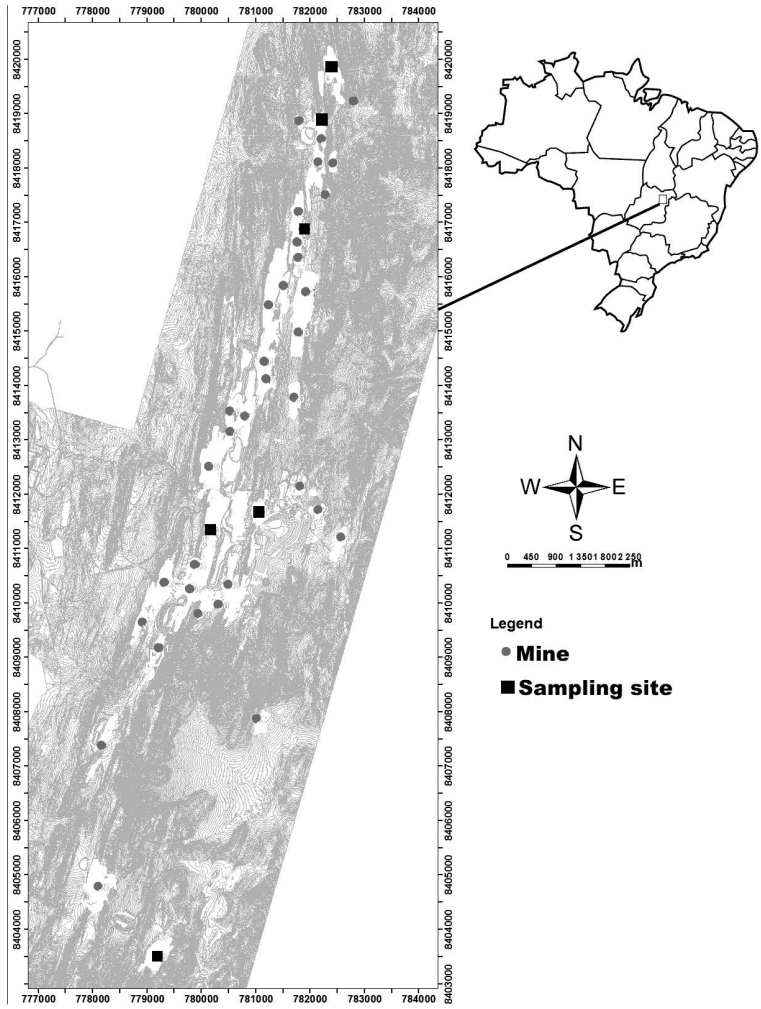

Figure 1. Topographic and sampling-site map of Niquelândia, Brazil (image courtesy of Votorantim Metais Níquel).

silicated ore types, seven samples were collected throughout the deposit (Figure 1). Chemical analyses of the bulk samples were performed using inductively coupled plasma-atomic emission spectroscopy (ICP-AES) for the main elements (Mg, Si, Fe, Ni, Al, Cu, Co, Mn, and Cr) and confirmed the broad chemical variability, especially for NiO and Fe_2O_3. Loss on ignition (LOI) was also measured.

Sample AS-ANi3 represents a partially altered peridotite with large amounts of NiO (lowermost part of the weathering profile). Sample ASL-I5 corresponds to the intensely altered part of the profile (uppermost), near the oxidized zone, which results in large Fe_2O_3 contents. Samples from peridotites located near quartz veins, such as AS-BNi2, contain low grades of NiO. The other samples have intermediate amounts of Ni and Fe, varying according to their location in the weathering profile.

In order to identify the clay minerals, the <2 μm fraction was extracted from each of the bulk samples. Initially, the samples were dispersed in distilled water. The fine fractions (<50 μm) were separated from coarse material (>50 μm) by wet sieving. The coarse fractions were discarded. The fine fractions (<50 μm) were saturated with 1 mol L^{-1} NaCl (Moore and Reynolds, 1989) to deflocculate the particles. The clay fraction (<2 μm) was obtained by centrifugation (according to Stokes' law). A proportion of the <2 μm fraction of each sample was subsequently flocculated and saturated with 0.5 mol L^{-1} $CaCl_2$. Ca-saturated clay fractions were washed with distilled water to remove excess salts. The remainder was kept in suspension for extraction of <0.1 μm fractions.

Oriented preparations of Ca-saturated <2 μm fractions were obtained by depositing clay suspensions on glass slides which were dried at room temperature (air-dried: AD) and also saturated with ethylene glycol (EG) vapor at 50ºC for 16 h.

In order to distinguish high- from low-charge smectites, the Ca/K/Ca sequence of saturation was carried out

https://doi.org/10.1346/CCMN.2014.0620406 Published online by Cambridge University Press

(Calarge *et al.*, 2003). First, the samples were saturated with 0.5 mol L^{-1} $CaCl_2$, followed by 1 mol L^{-1} KCl; then, a further Ca saturation step was performed. Ultimately, the samples were washed to eliminate the excess salts. Smectites with high tetrahedral charge remained collapsed at ~10 Å in AD and EG states, whereas smectites with low tetrahedral charge re-expanded to ~15 Å in AD and ~16–17 Å in EG states, once Ca replaced K in the last saturation step. For samples AS-ANi3, VSL-R2, and ASL-AN3, the <0.1 μm fractions were obtained by repeated centrifugation cycles until the supernatant became clear. Later, the fractions were Ca-saturated and prepared using the same procedure as adopted for the <2 μm fractions.

Lithium saturations were performed to characterize the octahedral (Oc) and tetrahedral (Te) locations of the charge (*e.g.* Hofmann and Klemen, 1950). Samples were saturated with 1 mol L^{-1} LiCl and washed with ethanol to remove the excess salts; they were then heated overnight at 300ºC. The first step involved a complete exchange of the interlayer cations by Li^+ and the second step involved migration of the Li^+ to the octahedral vacancies of the dioctahedral smectites and, consequently, neutralization of the octahedral layer charge. The swelling properties of the clays are affected in different ways, depending on the layer charge and on the location of the charge. According to Petit *et al.* (2002) and Gaudin *et al.* (2004a), layers having tetrahedral charge of <0.18 per half unit cell do not swell following the Hofmann-Klemen (HK) treatment and EG solvation, whereas layers with tetrahedral charge >0.18 per half unit cell are expandable. For trioctahedral smectites with octahedral charge, Li-saturation followed by heating (HK treatment) results in only partial neutralization and compensates approximately half of the charge (Li^+ *vs.* Mg^{2+} or Ni^{2+}) and the layers remain expandable (Petit *et al.*, 2008).

X-ray diffraction (XRD) patterns for oriented preparations were recorded using a Bruker D8 Advance diffractometer (CuKα radiation, 40 kV, 40 mA, Lynxeye detector) from 2.5 to 35º2θ in 0.012º2θ steps and a counting time per step of 96 s. The XRD patterns were obtained from oriented Ca-saturated clay in AD and EG states, oriented Ca/K/Ca saturations in AD and EG states, and after Li-saturated preparation, in AD and EG states, heated overnight at 300ºC ($Li_{300}H$) and followed by solvation with EG ($Li_{300}H$ EG).

The $d_{06\text{-}33}$ on randomly oriented powders of <2 μm fractions were used to distinguish between di- and trioctahedral clay minerals. The samples were prepared using the back-loading procedure (Moore and Reynolds, 1989). Powder XRD patterns were obtained by scanning from 57 to 63º2θ in 0.02º2θ steps at 96 s/step. The *HighScore Plus*® software (PANanalytical/Spectris, Netherlands) was used to analyze the patterns.

Microanalyses were performed by EDX (energy dispersive X-ray spectroscopy) (INCA, Oxford, UK) using 20 kV with SDD (silicon drift detector), coupled to a scanning electron microscope (SEM) (LEO-Stereoscan 440 from Leica). A JEOL JSM-5600LV coupled to a BRUKER X-Flash 4010 EDS spectrometer was also used to analyze the <2 μm powders. The EDX microanalyses of the clay particles were plotted on ternary diagrams to compare the different smectite compositions.

Fourier-transform infrared (FTIR) spectroscopy was used to constrain the crystal chemistry of the Fe-Ni smectites studied as well as to further refine the layer-charge distribution using ammonium saturations (Petit *et al.*, 1998). Mid-infrared (MIR) analyses were performed using a Nicolet Magna-IR 760 spectrometer in the 400–4000 cm^{-1} range with a 2 cm^{-1} resolution. The spectra were obtained from pressed KBr pellets, prepared by mixing 1 mg of sample with 150 mg of KBr and pressing at 10 t cm^{-2} and drying overnight at 110ºC. Near-infrared (NIR) spectra from 4000 to 10,000 cm^{-1} were obtained at a resolution of 4 cm^{-1} on powder in glass vial, using a Thermo Scientific Integrating Sphere (diffuse reflectance) with an internal InGaAs detector coupled to a Thermo Scientific Nicolet 6700 FTIR spectrometer.

Before and after Li treatment, the samples were saturated with 1 mol L^{-1} NH_4Cl five times and washed with ethanol until free of NH_4 salts. This procedure was performed to quantify the amounts of NH_4^+ in the NH_4-saturated smectites. The detailed procedure was given by Petit *et al.* (1998, 2006). The NH_4^+ fixed by the bulk smectites corresponds to the total layer charge (permanent Te + Oc + variable edge charges), *i.e.* the cation exchange capacity (CEC) (at the pH of the NH_4Cl solution). After Li saturation and heating for 16 h at 300ºC (Hofmann-Klemen treatment), the amount of NH_4^+ adsorbed corresponds to the remaining charge after neutralization by Li fixation. As a result, the difference between them was attributed to the neutralized charge by the Li treatment, *i.e.* the octahedral charge for the dioctahedral smectites (montmorillonites) and half of the octahedral charge for the trioctahedral smectites (stevensite) as described by Petit *et al.* (2008). The IR spectra of NH_4^+-saturated samples (NH_4^+ and $Li_{300}NH_4$) were recorded using the same amount of clay and they were normalized to the main SiO band around 1020 cm^{-1} using *Omnic*® software (Thermo Fisher Scientific Inc, United States) as the samples contain both dioctahedral and trioctahedral smectites and are devoid of quartz. The integrated intensity of the NH_4 deformation (υ_4NH_4) band at 1400 cm^{-1} was measured before and after Li treatment (area: ANH_4; range 1353–1500 cm^{-1}) in arbitrary units using the *Omnic*® software. The surface area of the υNH_4 band (after normalization) was correlated to the CEC of the sample (Petit *et al.*, 1998, 2002, 2008; Gaudin *et al.*, 2005). The ratio of the integrated intensity of $ALi_{300}NH_4/ANH_4$ corresponded to the percentage of the charge remaining after Li treatment.

https://doi.org/10.1346/CCMN.2014.0620406 Published online by Cambridge University Press

Table 1. Chemical composition (wt.%) determined using ICP-AES, for all samples.

Samples	NiO	Fe_2O_3	Al_2O_3	MgO	SiO_2	Cr_2O_3	LOI
AS-BNi2	2.11	17.7	3.95	4.87	51.0		8.45
AS-ANi3	23.4	5.23	2.45	7.44	39.9		6.82
ASL-I5	1.16	32.4	4.76	5.07	44.6	1.96	6.68
VSL1A	9.60	10.9	8.52	7.45	44.1	2.39	7.91
VSL-R2	4.74	10.1	3.93	19.1	35.1	1.08	3.71
ASL-AN3	7.75	13.4	5.07	12.4	40.1	1.33	5.53
CSL-G8	2.08	15.3	5.07	10.5	50.7	1.39	

RESULTS

Chemical analyses

The chemical compositions (main elements) of the bulk samples are shown in Table 1. Samples with abundant SiO_2 and LOI between 6 and 8 wt.% suggest the presence of clay minerals. High abundances of NiO (23.4%) for sample AS-ANi3 and Fe_2O_3 (32.4%) for sample ASL-I5 were measured. The samples VSL-R2 and ASL-AN3 contained 4.7 and 7.7% of NiO and 19.1% and 12.4% of MgO, respectively. The sample VSL1A had similar amounts of NiO and Fe_2O_3 (10−11%) and the largest Al_2O_3 content (8.5%). Finally, AS-BNi2 and CSL-G8 contained 17.7 and 15.3% Fe_2O_3, respectively, and a small amount of NiO and Al_2O_3 ($\leqslant$5%). Sample AS-BNi2 contained <5% MgO, whereas CSL-G8 had 10.5% MgO.

X-ray diffraction

The XRD patterns of the Ca-saturated clay fraction of the different samples were similar and showed a main peak at $d_{001AD} \approx 15$Å that expanded to $d_{001} \approx 16.5$ Å following the EG solvation (Figure 2). The peak at 8.3 Å was attributed to the 002 reflection of glycolated smectite. The peaks in the AD and EG states were symmetrical and the samples exhibited uniform swelling, supporting the presence of pure smectite layers and the absence of mixed layers with swelling and non-swelling layers in the different samples.

Powder XRD patterns exhibited asymmetrical *hk* reflections that are characteristic of turbostratic stacking of layers typical of smectites. The samples AS-BNi2, ASL-AN3, ASL-I5, CSL-G8, and VSL1A revealed $d_{06\text{-}33}$ values which varied from 1.50 to 1.51 Å (Figure 3) indicating that they consist essentially of dioctahedral Fe-rich smectites as described, for example, by Desprairies (1983), Petit *et al.* (1992), and Gaudin *et al.* (2004a, 2004b). The samples VSL-R2 and AS-ANi3 exhibited a large $d_{06\text{-}33}$ peak (Figure 3) probably due to the possible overlapping of different smaller peaks that hinder the identification of the di- or trioctahedral

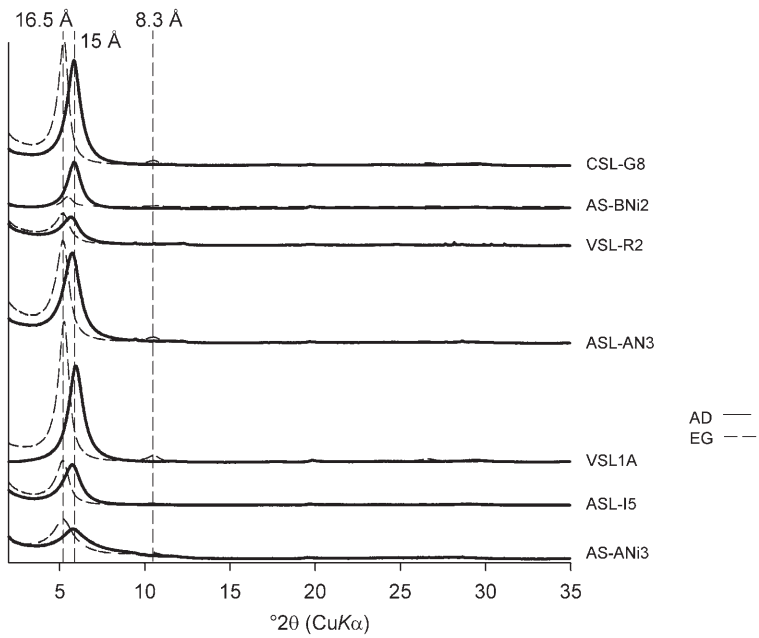

Figure 2. XRD oriented patterns of the <2 μm fraction for the Ca-saturated samples. AD: air-dried state (solid lines); EG: ethylene glycol-treated (dashed lines).

https://doi.org/10.1346/CCMN.2014.0620406 Published online by Cambridge University Press

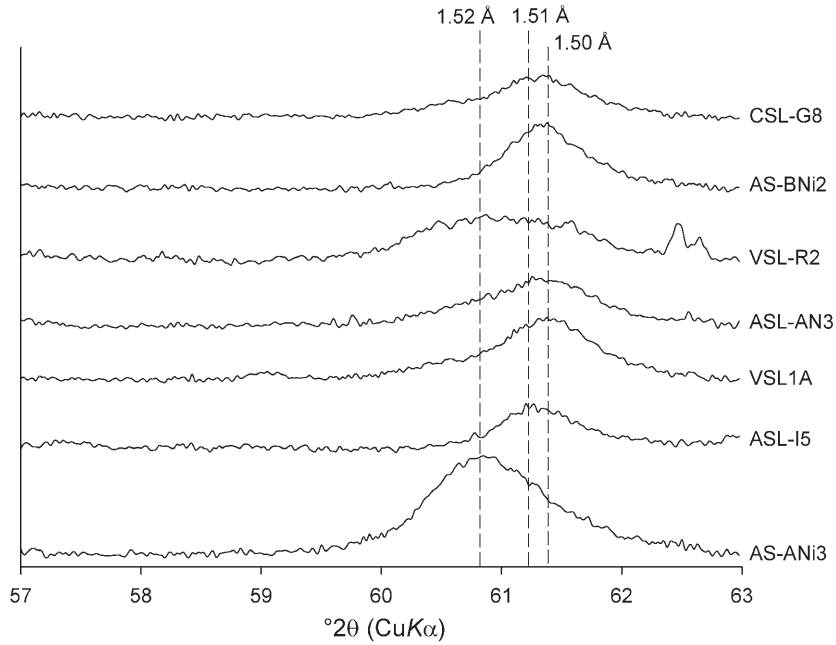

Figure 3. $d_{06\text{-}33}$ reflections. VSL-R2 presents a large $d_{06\text{-}33}$ peak attributed to mixtures of di- and trioctahedral smectites. AS-ANi3 consists essentially of trioctahedral smectites, whereas ASL-I5 consists of entirely of dioctahedral smectites.

character. Sample AS-ANi3 ($d_{06\text{-}33}$ = 1.52 Å), however, appeared to belong to the trioctahedral type, whereas VSL-R2 showed a mix of di- and trioctahedral mineral characteristics.

Following K^+ saturation, all the samples collapsed from 10.8–12.4 Å (AD) to 9.5–9.9 Å after heating at 550ºC (patterns not shown). The XRD patterns for Ca/K/Ca samples were very close to those of the Ca-saturated samples (not shown) suggesting a rather small tetrahedral charge of the layers for all of the samples, as K is replaced by Ca in the third saturation step.

The layer-charge distribution was determined by the HK procedure (Figure 4). The XRD patterns after HK treatment indicated a collapse of the layers between 9.3 and 9.6 Å. Following EG solvation, the 001 and 002 reflections broadened and the d_{001} values varied between 16 and 16.7 Å for different samples. For samples VSL-R2 and CSL-G8, HK swelling was almost complete for all layers after EG solvation. For most of the samples, however, the different d spacings and non-harmonic d_{001} and d_{002} values indicated different swelling behaviors that are related to the presence of HK-swelling and HK-non-swelling layers (random mixed layers). The smectites from Niquelândia have a heterogeneous layer-charge distribution, therefore, within the same population and between different samples, making it difficult to

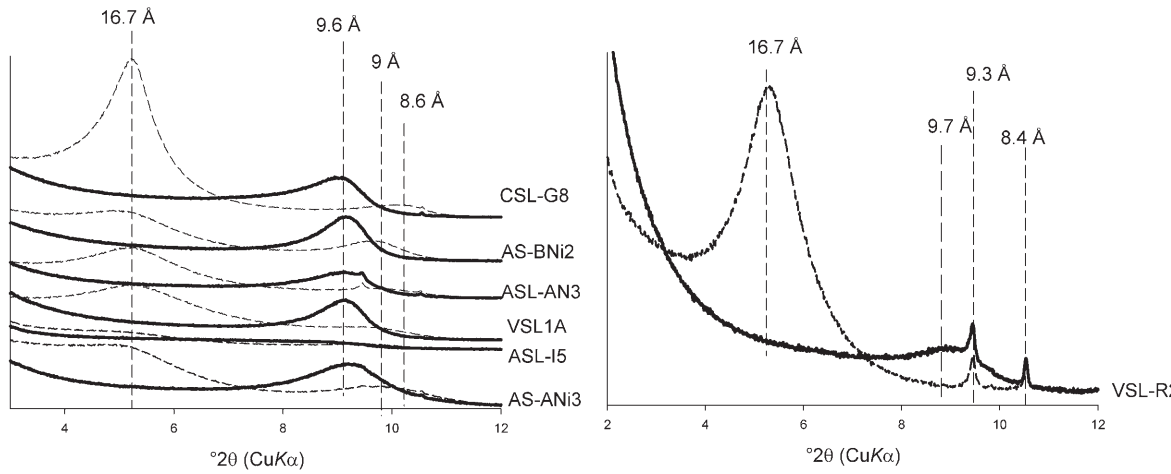

Figure 4. XRD patterns of samples after Hofmann-Klemen treatment. The solid lines correspond to $Li_{300}H$ and the dashed lines to $Li_{300}HEG$ samples, respectively.

https://doi.org/10.1346/CCMN.2014.0620406 Published online by Cambridge University Press

further refine the distribution of the layer charge from these XRD measurements.

Infrared results

Three categories of samples were differentiated by MIR spectroscopy: dioctahedral samples (ASL-I5, CSL-G8, and AS-BNi2 – Group A), trioctahedral samples (AS-ANi3 – Group B) and a mixture of these two types (VSL-R2, ASL-AN3, and VSL1A – Group C).

Dioctahedral samples ASL-I5, CSL-G8, and AS-BNi2 (Group A) consist mainly of dioctahedral smectites with a small amount of trioctahedral clays. In the OH-bending region, the bands at 820 cm^{-1} and at ~765 cm^{-1} (Figure 5) were assigned to $\delta Fe^{3+}Fe^{3+}OH$ and to $\delta Fe^{3+}MgOH$ (and/or maybe $\delta Fe^{3+}NiOH$), respectively, and the band at 870 cm^{-1} was attributed to $\delta AlFe^{3+}OH$ (Farmer, 1974; Petit *et al.*, 2002; Bishop *et al.*, 2002; Gaudin *et al.*, 2004a, 2004b, 2005).

In the OH-stretching region (Figure 5), the wide band at ~3555 cm^{-1} was attributed to $\upsilon Fe^{3+}Fe^{3+}OH$ superimposed on the $\upsilon Fe^{3+}MgOH$ band at 3575 cm^{-1} (Farmer, 1974; Wilson, 1994; Petit *et al.*, 2002; Petit, 2005; Gaudin *et al.*, 2004a, 2004b, 2005; Gates, 2005; Decarreau *et al.*, 2008; Andrieux and Petit, 2010). These features are characteristic of Fe-rich montmorillonites with Mg (and/or probably Ni) in the octahedral sites and indicate that Fe, Mg (and/or probably Ni) may occur in adjacent octahedral sites responsible for the heterogeneity of the samples. The IR spectra of Niquelândia dioctahedral smectite (ASL-I5, CSL-G8, AS-BNi2 – Figure 5) are very similar to the Fe-montmorillonite characterized in weathered ultrabasic nodules in Ölberg, Germany (Köster *et al.*, 1999; Petit *et al.*, 2002) or in pyrite-bearing calcareous sediments in the Costa Rica margin (Gaudin *et al.*, 2005).

Trioctahedral sample AS-ANi3 (Group B) consists mainly of trioctahedral Ni-smectites. Bands at 3624 cm^{-1} and 710 cm^{-1} (Figure 5) were assigned to νNi_3OH and δNi_3OH, respectively, as described for kerolite and talc (Wilkins and Ito, 1967; Farmer, 1974; Gerard and Herbillon, 1983; Petit, 2005; Christidis and Mitsis, 2006). This is in agreement with the large Ni content determined by chemical analysis.

Samples VSL-R2, ASL-AN3, and VSL1A (Group C) correspond to the mixture of dioctahedral and trioctahedral smectites described above and thus showed the characteristic bands of both smectite groups.

The NIR spectra corroborated the MIR results. A narrow band at 7185 cm^{-1} (Figure 6) was assigned to the $2\upsilon Mg_3$-OH vibration of talc (Petit *et al.*, 2004; Petit, 2005; Madejová *et al.*, 2011), for samples AS-ANi3 and VSL-R2.

Layer-charge reduction by Li treatment

The IR spectra of all samples (but to a lesser extent in sample AS-ANi3) are affected by the HK treatment (Figures 7, 8).

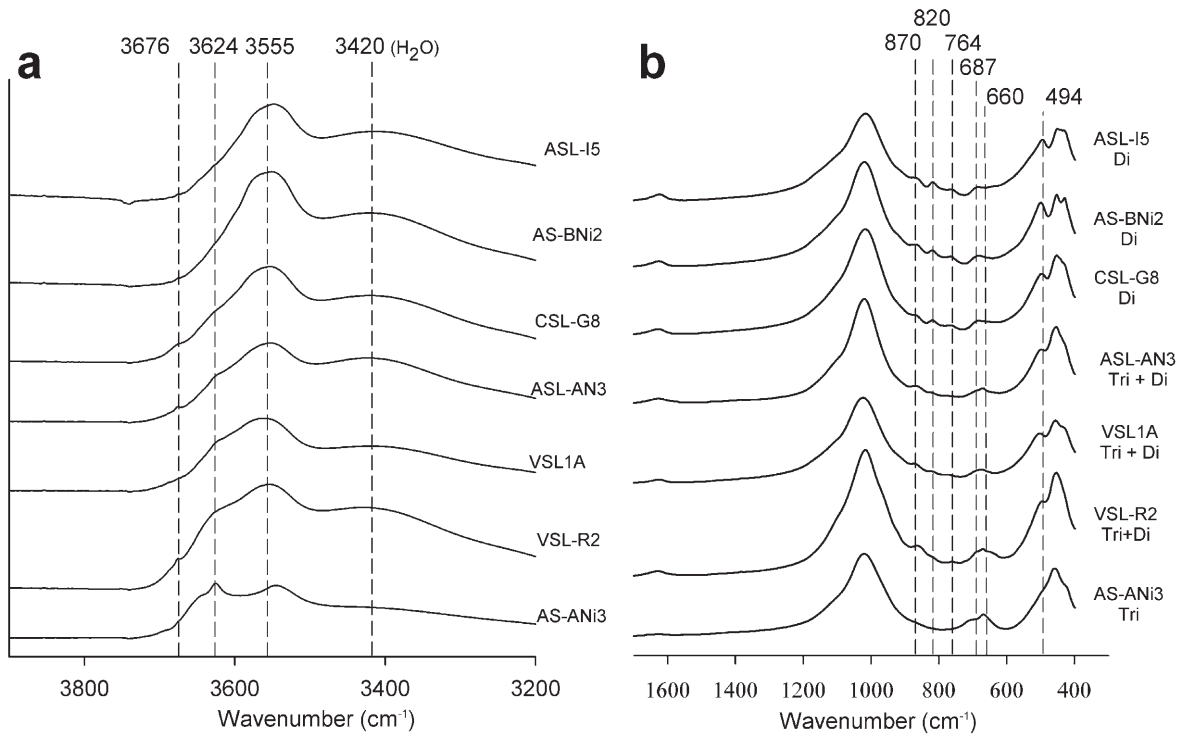

Figure 5. MIR spectra of all samples: VSL1A, ASL-AN3, VSL-R, AS-ANi3, AS-BNi2, CSL-G8, and ASL-I5. (a) The Ni-rich trioctahedral smectites present bands at 3624 cm^{-1} attributed to υNi_3OH. (b) The Fe-rich smectites present bands at 870 and 820 cm^{-1}, related to $\delta AlFe^{3+}OH$ and $\delta Fe^{3+}Fe^{3+}OH$, respectively.

https://doi.org/10.1346/CCMN.2014.0620406 Published online by Cambridge University Press

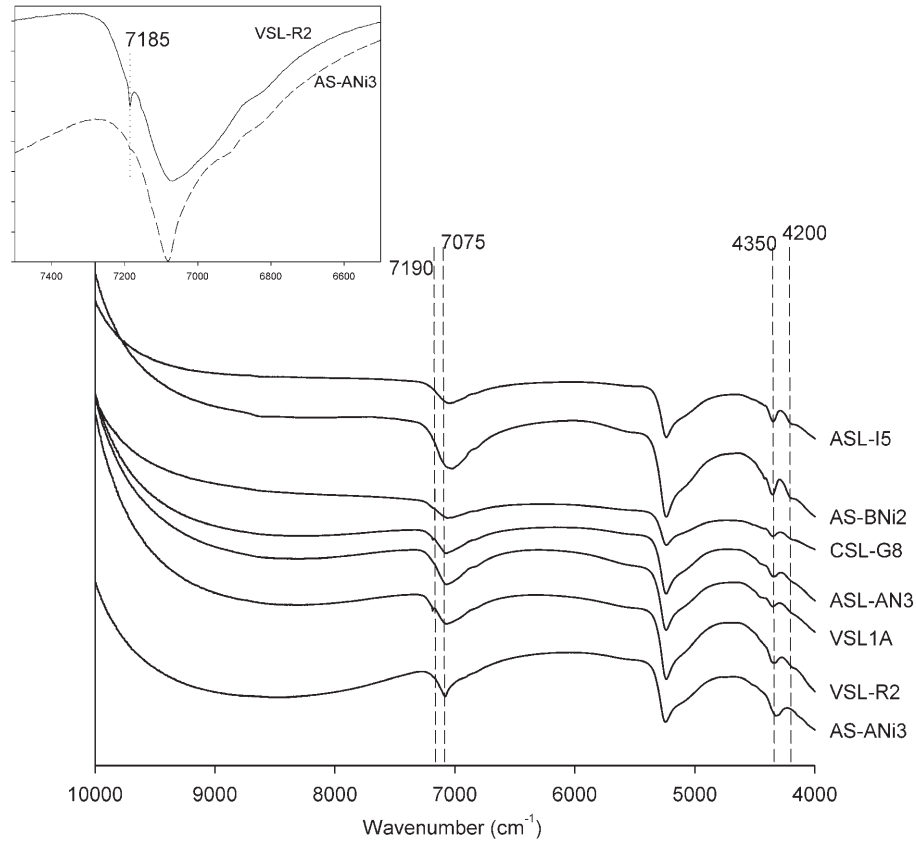

Figure 6. NIR spectra of samples VSL-R2, ASL-AN3, AS-ANi3, AS-BNi2, CSL-G8, VSL1A, and ASL-I5. The characteristic band for talc, at 7185 cm^{-1}, is noted.

For the dioctahedral samples, the structural changes after Li treatment were similar to those described for the Ölberg sample (Petit *et al.*, 2002). In the OH-stretching region, the bands at 3675 cm^{-1}, 3645 cm^{-1}, and the shoulder at ~3600 cm^{-1} were observed after Li saturation (Figure 6). They were attributed to

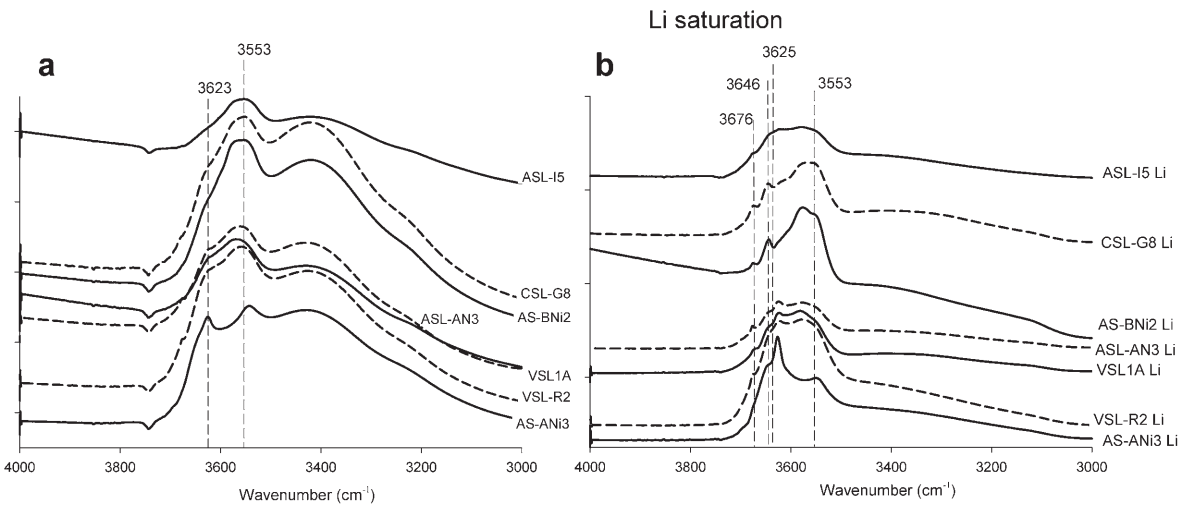

Figure 7. MIR spectra (range: 3000–4000 cm^{-1}) of bulk samples (a) and after HK treatment (b) for samples VLS1A, ASL-AN3, VSL-R2, AS-ANi3, AS-BNi2, CSL-G8, and ASL-I5. New bands were observed after Li treatment (3675 cm^{-1}, 3645 cm^{-1}, and a shoulder at 3600 cm^{-1}).

https://doi.org/10.1346/CCMN.2014.0620406 Published online by Cambridge University Press

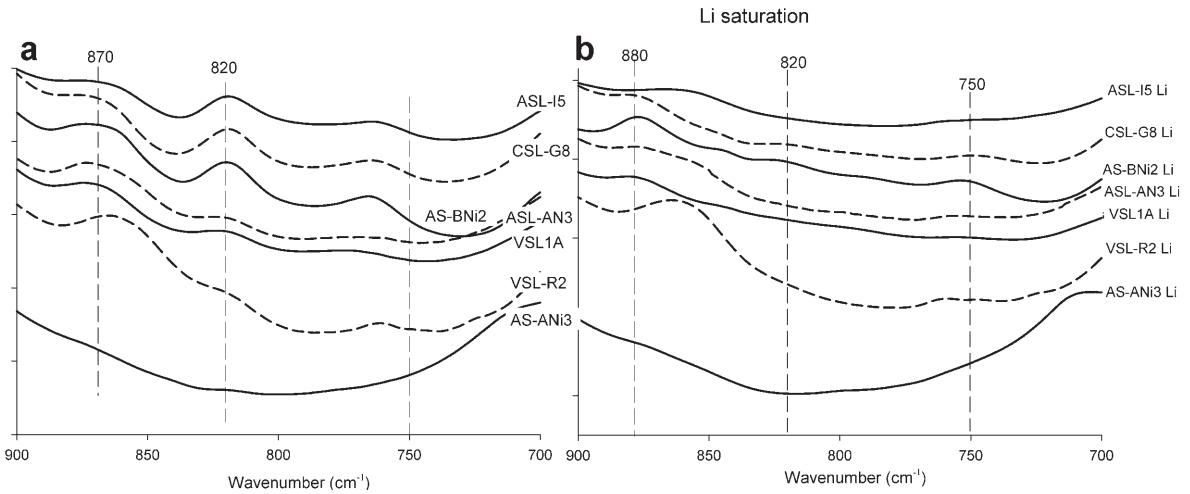

Figure 8. MIR spectra (range: 1000–400 cm^{-1}) of bulk samples (a) and after HK treatment (b) for samples VSL1A, ASL-AN3, VSL-R2, AS-ANi3, AS-BNi2, CSL-G8, and ASL-I5.

υLiR^{2+}OH vibrations (R being Mg^{2+}, Fe^{3+} or Ni^{2+}) by Petit *et al.* (2002) and Gaudin *et al.* (2005). In addition, the intensity of the band at 3555 cm^{-1} decreased. In the OH-bending region, structural changes were also observed (Figure 8). After Li treatment, the δAlFe^{3+}OH band at 870 cm^{-1} shifted to 880 cm^{-1}, the intensity of the band at 820 cm^{-1} (δ$Fe^{3+}Fe^{3+}$OH) decreased, and a band appeared at 750 cm^{-1} (AS-BNi2Li). The latter band is attributed to the trioctahedral domains created by the migration of Li into the vacant sites (Petit *et al.*, 2002).

For the trioctahedral samples, the changes in IR spectra after Li treatment were more subtle as observed by Petit *et al.* (2008) for synthetic Zn-stevensite.

The decrease in layer charge after Li treatment was obtained from the decrease in the integrated intensity of the $υ_4NH_4$ band at 1400 cm^{-1} (Figure 9, Table 2) showing about half of the CEC (44% for VSL-R2 and 63% for CSL-G8) determined for the <2 μm fraction of all the samples. For dioctahedral smectites, the remaining charge not neutralized by Li^+ was attributed to tetrahedral plus variable charges. For trioctahedral smectites (*e.g.* AS-ANi3), the remaining charge was ~50% of the total layer charge, consistent with the 50% neutralization of the octahedral charge by Li^+ in the stevensite structure ($[NH_4]_{2x}Si_4[Mg, Ni]_{3-x}□_xO_{10}[OH]_2$ → $[NH_4]_xSi_4[Mg, Ni]_{3-x}<Li>_xO_{10}[OH]_2$; □ being a vacancy), as described by Petit *et al.* (2008) for synthetic Zn-stevensite.

The CEC values for samples ASL-I5 and AS-ANi3, measured independently using the ammonium acetate method, were 81 and 41 meq/100 g, respectively. Using these values and integrated intensities of the 1400 cm^{-1} band of the NH_4-saturated samples, the CEC of the other samples was estimated (Petit *et al.*, 1998). The CEC of the <2 μm fractions ranged from 41 (AS-ANi3) to 100 meq/100 g (AS-BNi2) (Table 2). The <2 μm and <0.1 μm fractions of sample AS-ANi3 revealed the same

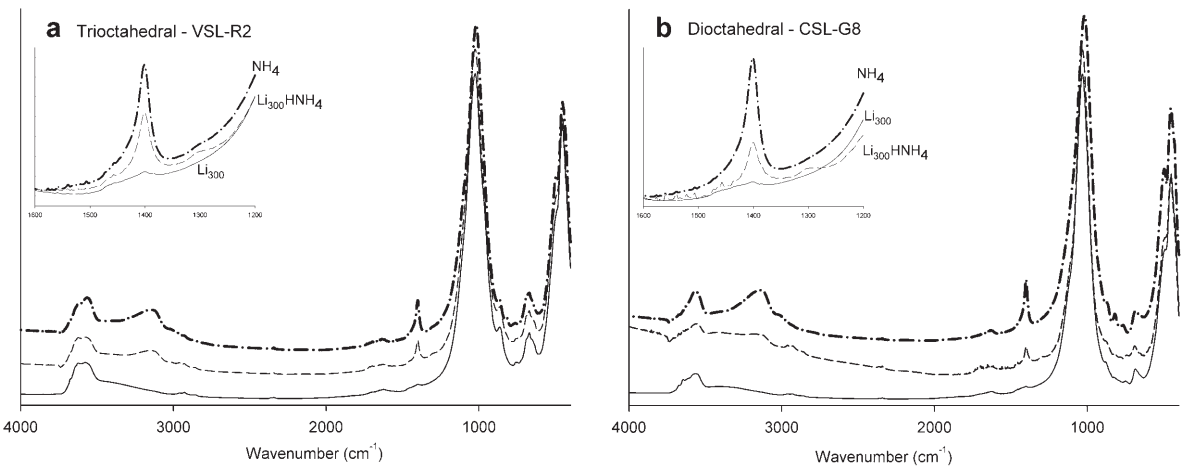

Figure 9. MIR spectra for samples VSL-R2 (a) and CSL-G8 (b): Li_{300} (solid line), $Li_{300}HNH_4$ (dashed line), and NH_4 (dash-dot line).

https://doi.org/10.1346/CCMN.2014.0620406 Published online by Cambridge University Press

Table 2. CEC and octahedral charge obtained for Niquelândia smectite samples.

Samples	AS-BNi2 Di	AS-ANi3 Tri		ASL-I5 Di	VSL-R2 Di+Tri		CSL-G8 Di	VSL1A Di+Tri	ASL-AN3 Di+Tri	
Size (μm)	<2	<2	<0.1	<2	<2	<0.1	<2	<2	<2	<0.1
CEC (meq/100 g)	100	41	39	81	60	77	79	83	67	89
Ratio of charge neutralized by Li^+ (%)	55	48	52	57	44	71	63	54	49	69

CEC and origin of charge (Table 2). This is in agreement with the similarity of the FTIR spectra for both size fractions (Figure 10). In contrast, for samples VSL-R2 and ASL-AN3, which are mixtures of di and trioctahedral smectites, the CEC and the origin of charge varied significantly between the <2 μm and <0.1 μm fractions, with a larger CEC value and higher ratio of charges neutralized by Li^+. In fact, the FTIR spectra of the two fractions of these samples revealed that the <0.1 μm fractions are relatively enriched in Fe-montmorillonite compared to the <2 μm fractions with a relative increase in the band at 820 cm^{-1} and an increase in the band at 670−710 cm^{-1} (trioctahedral smectites).

Scanning electron microscopy

The typical morphology of smectites, honeycomb structure and wavy flakes (Figure 11), was observed in the Ni-rich sample (AS-ANi3) and in the Mg-rich sample (VSL-R2).

The SEM-EDX microanalysis data of the K-saturated <2 μm fractions plotted in ternary diagrams (Figure 12) revealed chemical heterogeneities for the different samples. Sample AS-ANi3 contains a remarkable amount of Ni (31 ± 2.4%; Figures 12b and 12c) and corresponds to the trioctahedral Ni-rich stevensite end-member (Figure 12a). The samples ASL-I5 and AS-BNi2 are enriched in Fe (Figures 12b and 12c) and correspond to the dioctahedral end-member (Fe-montmorillonite) (Figure 12a). Samples CSL-G8, VSL1A, VSL-R2, and ASL-AN3 have chemical compositions intermediate between the two end-members described above (Figure 12b,c).

For samples VSL-R2 and ASL-AN3, the oriented trend toward the Mg pole (Figure 12d) may be attributable to the presence of talc as revealed by other techniques.

The average structural formulae of the two di- and trioctahedral end-members of the Niquelândia smectites were estimated roughly from powder analyses of samples ASL-I5 and AS-ANi3 based on 11 oxygens, expressing Fe as Fe^{3+}, and taking into account FTIR structural data (Table 3). The octahedral charge was adjusted to take into account the results of FTIR and $Li_{300}H$-NH_4 saturations.

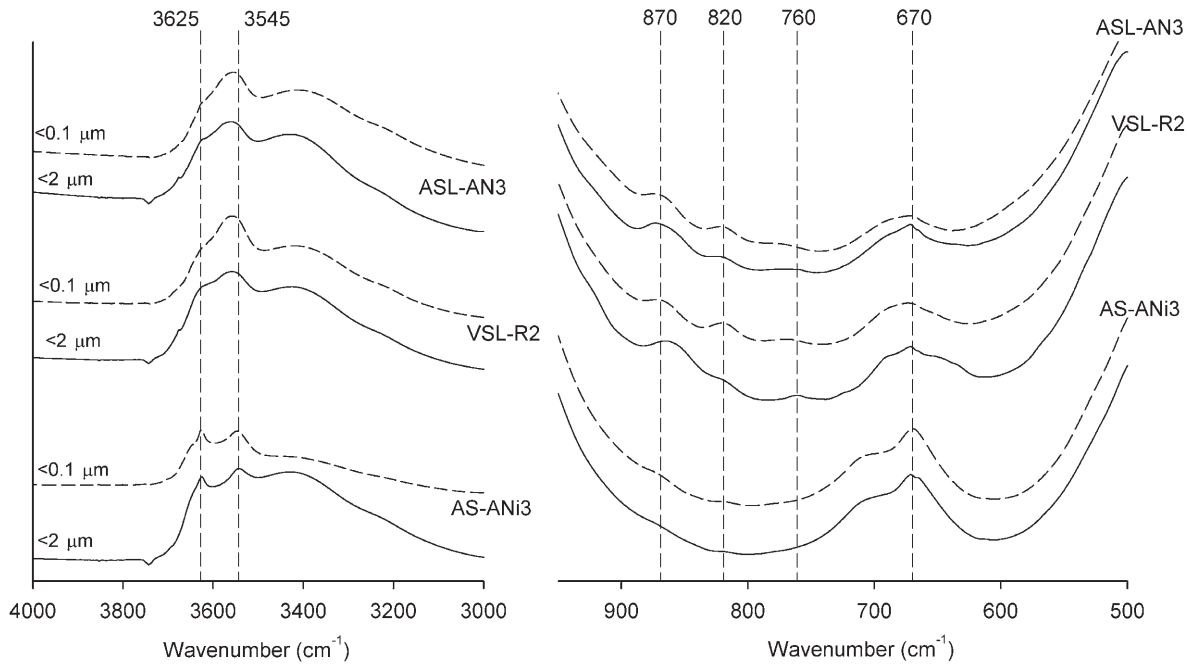

Figure 10. MIR spectra of the <2 μm (solid line) and <0.1 μm fractions (dashed line) of samples AS-ANi3, VSL-R2, and ASL-AN3.

https://doi.org/10.1346/CCMN.2014.0620406 Published online by Cambridge University Press

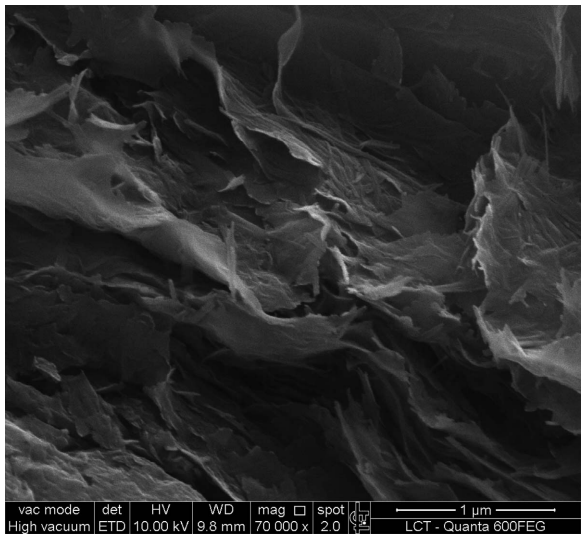

Figure 11. SEM-SE (secondary electron) image of smectite in sample VSL-R2 with typical wavy-flake particles.

The dominant octahedral cation of the dioctahedral end-member is Fe^{3+} (1.50 atoms per half unit cell), which is in the range of values obtained by Petit *et al.* (2002) and Gaudin *et al.* (2004a) for Fe-montmorillonites. For trioctahedral smectites, the dominant octahedral cation is Ni (>2 atoms per half unit cell).

DISCUSSIONS AND CONCLUSIONS

The results for the <2 µm fractions confirmed that most of the samples are formed by mixtures of Fe-montmorillonite and Ni-stevensite with traces of talc for some samples.

The calculated structural formulae (Table 3) obtained by EDX and FTIR analysis show that there is no chemical substitution in tetrahedral sheets for trioctahedral smectites (AS-ANi3). For dioctahedral smectites, Si^{4+} is replaced by Al^{3+} in small proportions (0.14 atoms per half unit cell).

With respect to the octahedral sheet, the Ni^{2+} is the dominant cation for trioctahedral smectites, reaching 2.2 Ni atoms per half unit cell. Ni-rich smectites are rare in

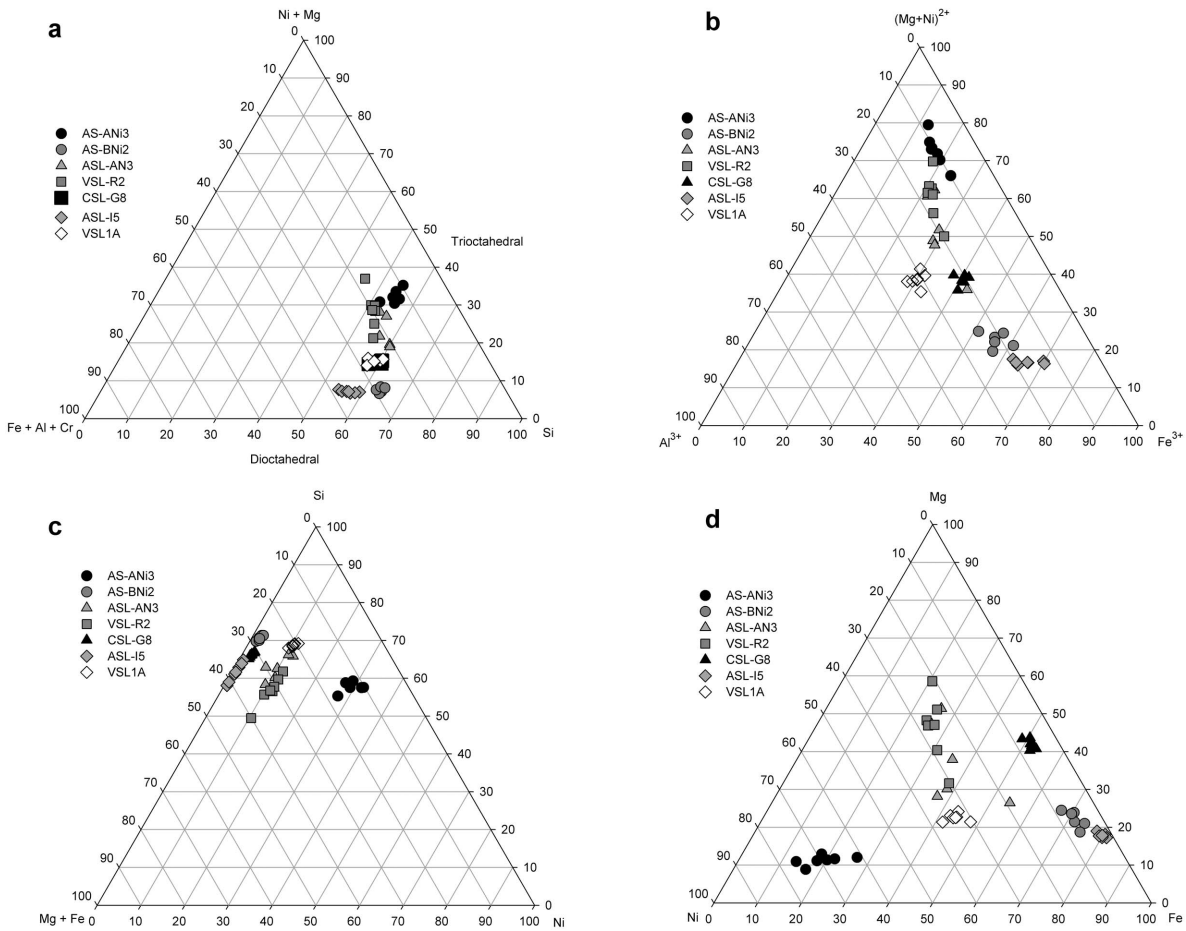

Figure 12. SEM-EDX microanalysis of K-saturated powders plotted in ternary diagrams (atom.%).

https://doi.org/10.1346/CCMN.2014.0620406 Published online by Cambridge University Press

Table 3. Structural formulae of Niquelândia smectites (on the basis of 11 oxygens) from SEM-EDX analyses of powders of K-saturated samples. The layer-charge distribution is adjusted on the basis of FTIR data. Tri = AS-ANi3; Di+Tri = VSL-R2, VSL1A, and ASL-AN3; Di = ASL-I5.

		Di	Tri
IV	Si^{4+}	3.86	4
IV	Al^{3+}	0.14	0
IV	Fe^{3+}	0	0
VI	Al^{3+}	0.25	0
VI	Fe^{3+}	1.50	0.20
VI	Mg^{2+}	0.16	0.21
VI	Cr^{3+}	0.04	0.07
VI	Ni^{2+}	0.05	2.2
inter	K^{+}	0.31	0.33
Σ IV		4.00	4.00
ΣVI		2.17	2.69
Charge IV		−0.50	0
Charge VI		−0.66	0.33
Total charge		−1.15	0.33
% charge VI		57	100
% charge $Li_{300}H$		57	48

nature; a dioctahedral Ni-smectite which does not exceed 0.4 Ni atoms per half unit cell was studied by Bosio *et al.* (1975), Brindley and de Souza (1975), and Gaudin *et al.* (2004a). Only Christidis and Mitsis (2006) found a Ni-smectite in Othrys, Greece, with >2 Ni per half unit cell. For the dioctahedral smectites, Fe^{3+} is the dominant octahedral cation (1.5 Fe atoms per half unit cell). Niquelândia dioctahedral smectites show an over-occupancy of octahedral sheets (2.17 atoms p.h.f.u.).

Lithium saturations and structural formulae showed that the layer charge arises especially in octahedral sheets for most samples, confirming that Fe-montmorillonites are characteristic dioctahedral smectites in ultrabasic weathered rocks as described by Gaudin *et al.* (2004a, 2004b). Another Fe-rich octahedral charged smectite was also described in deep-sea pyrite-rich sediments (Gaudin *et al.*, 2005; Wiewióra *et al.*, 2001).

The samples AS-ANi3 and VSL-R2, located at the bottom of the profile, consist essentially of Mg and Ni-rich smectites and also of some preserved pyroxene grains, suggesting that Mg- and Ni-rich smectites were formed from alteration of peridotites and pyroxenite. A trioctahedral Mg-bearing smectite was observed (Oliveira, 1990; Nahon *et al.*, 1982; Colin *et al.*, 1990) to have formed by incongruent and congruent dissolution of olivines and pyroxenes. The olivine from the peridotites is a continuous source of Ni capable of replacing Mg in trioctahedral smectites. The intense weathering process and continuous Mg and Ni leaching transformed trioctahedral smectite into an Fe-rich dioctahedral smectite (Colin *et al.* 1990). This interpretation was confirmed by the infra-micrometric fractionation study that showed that Fe-montmorillonite coexists, at the smallest size (<0.1 μm), in the tri-octahedral Ni-Fe stevensite samples. This also agrees with the results of Decarreau and Bonnin (1986) who determined that a nontronite-like smectite formed from an Fe-stevensite in atmospheric oxidized conditions.

The great heterogeneity of Ni distribution in both dioctahedral and trioctahedral smectites seems to be responsible for the large variation in Ni recovery during ore processing. Differences in the clay-mineral structure due to chemical substitutions may require different ore behaviors during the leaching process. Likewise, for the same smectite, different dissolution rates for one sample treated with Li^{+} and another treated with Ni^{2+} were observed by Pálková *et al.* (2003) due to structural modifications.

ACKNOWLEDGMENTS

This study was supported by CAPES (Coordenação de Aperfeiçoamento de Pessoal de Nível Superior/Brazilian Coordination for the Improvement of Higher Education Personnel) – Project CAPES/COFECUB: 9075/12-7−Te 761/12 and FAPESP (Fundação de Apoio à Pesquisa do Estado de São Paulo/ the São Paulo State Research Foundation) – project 10/50849-4. The authors thank the Votorantim Metais Níquel Company for all their contributions. The authors also thank the editors and reviewers for their constructive reviews and careful editing of the manuscript.

REFERENCES

Andrieux, P. and Petit, S. (2010) Hydrothermal synthesis of dioctahedral smectites: The Al−Fe^{3+} chemical series: Part I: Influence of experimental conditions. *Applied Clay Science*, **48**, 5−17.

Bishop, J., Murad, E., and Dyar, M.D. (2002) The influence of octahedral and tetrahedral cation substitution on the structure of smectites and serpentines as observed through infrared spectroscopy. *Clay Minerals*, **37**, 617−628.

Bosio, N.J., Hurst, V.J., and Smith, R.L. (1975) Nickeliferous nontronite, a 15 Å garnierite, at Niquelândia, Goiás, Brazil. *Clays and Clay Minerals*, **23**, 400−403.

Brindley, G.W. and de Souza, J.V. (1975) Nickel-containing montmorillonites and chlorites from Brazil, with remarks on schuchardtite. *Mineralogical Magazine*, **40**, 141−152.

Calarge, L., Lanson, B., Meunier, A., and Formoso, M.L. (2003) The smectitic minerals in a bentonite deposit from Melo (Uruguay). *Clay Minerals*, **38**, 25−34.

Christidis, G.E. and Mitsis, I. (2006) A new Ni-rich stevensite from the ophiolite complex of Othrys, Central Greece. *Clays and Clay Minerals*, **54**, 653−666.

Coelho, A.C.V., Poncelet, G., and Ladrière, J. (2000) Nickel, iron-containing clay minerals from Niquelânida deposit, Brazil – 1 Characterization. *Applied Clay Science*, **17**, 163−181.

Colin, F., Noack, J., Trescases, J., and Nahon, D. (1985) L'altération latéritique débutante des pyroxénites de Jacuba, Niquelândia, Brésil. *Clay Minerals*, **20**, 93−113.

Colin, F., Nahon, D., Trescases, J.J., and Melfi, A.J. (1990) Lateritic weathering of pyroxenites at Niquelândia, Goias, Brazil: The supergene behavior of nickel. *Economic Geology*, **85**, 1010−1023.

Dalvi, A., Bacon, G., and Osborne, R. (2004) The past and the future of nickel laterites. Pp. 7−10 in: PDAC 2004

https://doi.org/10.1346/CCMN.2014.0620406 Published online by Cambridge University Press

International convention, Toronto, Canada. *Trade show and investors exchange*. Prospectors and Developers Association of Canada, Toronto.

de Oliveira, S.M.B. (1990) *Os depósitos de Níquel Lateríticos do Brasil*. PhD thesis, Universidade de São Paulo, Instituto de Geociências, São Paulo, Brazil.

De Souza, J.V., Santos, P.S., and Santos, H.S. (1978) Caracterização mineralógica de algumas argilas niquelíferas brasileiras. *Revista Cerâmica*, **24**, 434–446.

Decarreau, A. and Bonnin D. (1986) Synthesis and crystallogenesis at low temperature of Fe(III)-smectites by evolution of coprecipitated gels: Experiments in partially reducing conditions. *Clay Minerals*, **21**, 861–877.

Decarreau, A., Colin, F., Herbillon, A., Manceau, A., Nahon, D., Paquet, H., Trauth-Badaud, D., and Trescases, J.J. (1987) Domain segregation in Ni-Fe-Mg smectites. *Clays and Clay Minerals*, **35**, 1–10.

Decarreau, A., Petit, S., Martin, F., Farges, F., Vieillard, P., and Joussein, E. (2008) Hydrothermal synthesis, between 75 and 150ºC, of high-charge, ferric nontronites. *Clays and Clay Minerals*, **56**, 322–337.

Desprairies, A. (1983) Relation entre le paramètre b des smectites et leur contenu en fer et magnesium. Application à l'étude des sédiments. *Clay Minerals*, **18**, 165–175.

Farmer, V.C. (1974) *Infrared Spectra of Minerals*. Monograph **4**, The Mineralogical Society, London.

Gates, W.P. (2005) Infrared spectroscopy and the chemistry of dioctahedral smectites. Pp. 125–168 in: *The Application of Vibrational Spectroscopy to Clay Minerals and Layered Double Hydroxides* (J.T. Kloprogge, editor). CMS Workshop Lectures, **13**, The Clay Minerals Society, Aurora, Colorado, USA.

Gaudin, A., Grauby, O., Noack, Y., Decarreau, A., and Petit, S. (2004a) Accurate crystal chemistry of ferric smectites from the lateritic nickel ore of Murrin Murrin (Western Australia). I. XRD and multi-scale chemical approaches. *Clay Minerals*, **39**, 301–315.

Gaudin, A., Petit, S., Rose, J., Martin, F., Decarreau, A., Noack, Y., and Borschneck, D. (2004b) The accurate crystal chemistry of ferric smectites from the lateritic nickel ore of Murrin Murrin (Western Australia). II. Spectroscopic (IR and EXAFS) approaches. *Clay Minerals*, **39**, 453–467.

Gaudin, A., Buatier, M.D., Beaufort, D., Petit, S., Grauby, O. and Decarreau, A. (2005) Characterization and origin of Fe^{3+}-montmorillonite in deep-water calcareous sediments (Pacific Ocean, Costa Rica margin). *Clays and Clay Minerals*, **53**, 452–465.

Gerard, P. and Herbillon, A.J. (1983) Infrared studies of Ni-bearing clay minerals of the kerolite-pimelite series. *Clays and Clay Minerals*, **31**, 143–151.

Hofmann, U. and Klemen, R. (1950) Verlust der Austauschfähigkeit von Lithiuminonenan Bentonitdurch Erhitzung. *Zeitschrift für anorganische und allgemeine Chemie*, **262**, 95–99.

Köster, H.M., Ehrlicher, U., Gilg, H.A., Jordan, R., Murad, E. and Onnich, K. (1999) Mineralogical and chemical characteristics of five nontronite and Fe-rich smectites. *Clay Minerals*, **34**, 579–599.

Madejová, J., Balán, E., and Petit, S. (2011) Application of vibrational spectroscopy to the characterization of phyllosilicates and other industrial minerals. Pp. 171–226 in: *Advances in the Characterization of Industrial Minerals* (G.E. Christidis, editor). EMU Notes in Mineralogy, **9**, European Mineralogical Union and the Mineralogical Society of Great Britain and Ireland, London.

Marini, O.J., Fuck, R.A., Dardenne, M.A., and Danni, J.C.M. (1984) Província Tocantins – Setores Central e Sudeste. Pp. 205–264 in: *O pré-cambriano do Brasil* (F.F.M. de Almeida and Y. Hasui, editor). Edgard Blucher, São Paulo.

Moore, D.M. and Reynolds, R.C. Jr. (1989) *X-ray Diffraction and the Identification and Analysis of Clay Minerals*. Oxford University Press, New York.

Nahon, D., Colin, F., and Tardy, Y. (1982) Formation and distribution of Mg, Fe, Mn-smectites in the first stages of the lateritic weathering of forsterite and tephroite. *Clay Minerals*, **17**, 339–348.

Pálková, H., Madejová, J., and Righi, D. (2003) Acid dissolution of reduced-charge Li- and Ni-montmorillonites. *Clays and Clay Minerals*, **51**, 133–142.

Petit, S. (2005) Crystal-chemistry of talcs: a NIR and MIR spectroscopic approach. Pp. 41–64 in: *The Application of Vibrational Spectroscopy to Clay Minerals and Layered Double Hydroxides* (J.T. Kloprogge, editor). CMS Workshop Lectures Series, **13**, The Clay Minerals Society, Aurora, Colorado, USA.

Petit, S., Prot, T., Decarreau, A., Mosser, C., and Toledo-Groke, M.C. (1992) Crystallochemical study of a population of particles in smectites from a lateritic weathering profile. *Clays and Clay Minerals*, **40**, 436–445.

Petit, S., Righi, D., Madejová, J., and Decarreau, A. (1998) Layer charge estimation of smectites using infrared spectroscopy. *Clay Minerals*, **33**, 579–591.

Petit, S., Caillaud, J., Righi, D., Madejová, J., Elsass, F., and Köster, H.M. (2002) Characterization and crystal chemistry of an Fe-rich montmorillonite from Ölberg, Germany. *Clay Minerals*, **37**, 283–297.

Petit, S., Martin, F., Wiewióra, A., De Parseval, P., and Decarreau, A. (2004) Crystal-chemistry of talc: A near infrared (NIR) spectroscopy study. *American Mineralogist*, **89**, 319–326.

Petit, S., Righi, D., and Madejová, J. (2006) Infrared spectroscopy of NH_4^+-bearing and saturated clay minerals: A review of the study of layer charge. *Applied Clay Science*, **34**, 22–30.

Petit, S., Righi, D., and Decarreau, A. (2008) Transformation of synthetic Zn-stevensite to Zn-talc induced by the Hofmann-Klemen effect. *Clays and Clay Minerals*, **57**, 645–654.

Raous, S., Echevarria, G., Sterckeman, T., Hanna, K., Thomas, F., Martins, E.S., and Becquer, T. (2013) Potentially toxic metals in ultramafic mining materials: Identification of the main bearing and reactive phases. *Geoderma*, **192**, 111–119.

Wiewióra, A., Giresse, P., Petit, S., and Wilamowski, A. (2001) A deep-water glauconitization process on the Ivory Coast–Ghana marginal ridge (ODP site 959): determination of Fe^{3+}-rich montmorillonite in green grains. *Clays and Clay Minerals*, **49**, 540–558.

Wilkins, R.W.T. and Ito, J. (1967) Infrared spectra of some synthetic talcs. *American Mineralogist*, **52**, 1649–1661.

Wilson, M. (1994) *Clay Mineralogy: Spectroscopic and Chemical Determinative Methods*. Chapman & Hall, London.

(*Received 18 February 2014; revised 2 September 2014; Ms. 849; AE: R. Kukkadapu*)

https://doi.org/10.1346/CCMN.2014.0620406 Published online by Cambridge University Press